Electrostatic Interaction across a Single-Layer Carbon Shell

Stania, R ; Seitsonen, A P ; Kunhardt, D ; Büchner, B ; Popov, A A ; Muntwiler, M ; Greber, T

Abstract: Ions inside of fullerene molecules are model systems for the study of the electrostatic interaction across a single layer of carbon. For TbSc2N@C80 on h-BN/Ni(111), we observe with high-resolution X-ray photoelectron spectroscopy a splitting of the C 1s core level. The data may be explained quantitatively with density functional theory. The correlation of the C 1s eigenvalues and the Coulomb potential of the inside ions at the corresponding carbon sites indicates incomplete screening of the electric field due to the endohedral ions. The screening comprises anisotropic charge transfer to the carbon atoms and their polarization. This behavior is essential for the ordering of endohedral single-molecule magnets and is expected to occur in any single-layer material.

DOI: https://doi.org/10.1021/acs.jpclett.8b01326

Electrostatic Interaction across a Single Layer Carbon Shell

R. Stania,[†] A.P. Seitsonen,[‡] D. Kunhardt,[¶] B. Büchner,[¶] A.A. Popov,[¶]

M. Muntwiler,[§] and T. Greber[*,†]

†*Physik-Institut, Universität Zürich, CH-8057 Zürich, Switzerland*

‡*Département de Chimie, École Normale Supérieure, F-75005 Paris, France*

¶*Leibniz Institute of Solid State and Materials Research, D-01069 Dresden, Germany*

§*Paul Scherrer Institut, CH-5232 Villigen, Switzerland*

E-mail: greber@physik.uzh.ch

Abstract

Ions inside Fullerene molecules are model systems for the study of the electrostatic interaction across a single layer of carbon. For $TbSc_2N@C_{80}$ on h-BN/Ni(111) we observe with high-resolution x-ray photoelectron spectroscopy a splitting of the C 1s core level. The data may be explained quantitatively with density functional theory. The correlation of the C 1s eigenvalues and the Coulomb potential of the inside ions at the corresponding carbon sites indicates incomplete screening of the electric field due to the endohedral ions. The screening comprises anisotropic charge transfer to the carbon atoms and their polarisation. This behaviour is essential for the ordering of endohedral single molecule magnets and is expected to occur in any single layer material.

Graphical TOC Entry

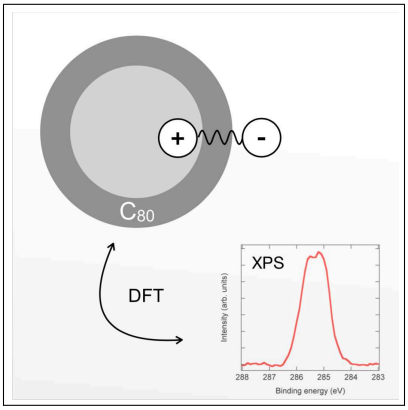

Keywords

Endofullerenes, dielectric constant, density functional theory, x-ray photoelectron spectroscopy

Introduction

Endohedral Fullerene molecules are carbon cages such as C_{60} or C_{80} that contain atoms. In the case of encapsulated paramagnetic atoms long spin coherence times[1] and single molecule magnetism have been observed.[2] The answer to the question whether Fullerenes match the picture of a Faraday cage[3] is important if for example the endohedral ordering is to be understood or if the magnetism shall be addressed with electric fields. Generally, electrostatic interaction with any single layer, as for example two dimensional graphene, affects the properties and performance of the material, and the interaction may also propagate across a single layer, which is an ultimate membrane that separates atoms in two volumes. For example, in the case of fluorinated graphene[4] one carbon atom in the two-atom unit cell undergoes a bond formation to fluorine in volume A and the other one to fluorine in volume B. This is due to a strong covalent C–F bond and the minimisation of steric repulsion. Interaction across a single layer is also expected in the case of non-covalently bound ionic species if their charge and magnetic moment is not completely screened. In the following we will investigate screening of electric fields of ions inside C_{80}. The dielectric constant is a descriptor of the screening of an electric field in a continuum that results in the polarisation of its surface. In graphene a dielectric constant has been deduced from the cyclotron mass. It depends on the charge carrier density and values from 2.2 to 4.9 have been inferred.[5] For bilayer graphene theory predicted a dielectric constant $\epsilon_\perp$ of ~ 3.[6] Strong local electric fields due to a point charge of an ion near atomically thin layers and the discreteness of the charges, may however impose charge transfer i.e. charging of the layer at the nanometer scale, which is different to the concept of polarisation of a dielectric.

Endohedral Fullerenes are model systems for the study of electrostatic interaction across a single layer of carbon, where the Fullerene cage takes the role of the carbon layer, and the endohedral unit acts as a source of the electric field. The facts that different endohedral clusters, such as $Tb_2ScN@C_{80}$ and $TbSc_2N@C_{80}$, may be separated with high pressure liquid chromatography, and the ordering of endohedral units in single crystals, prove that there is

interaction across the cage.[7,8] Further evidence for interaction across the cage or recognition of the interior and its conformation come from the observation of preferential orientation of endohedral units on copper,[9] and on rhodium, where concomitant magnetic ordering was observed.[10]

For C_{80} it is known that nominally 6 electrons have to be transferred to the carbon atoms for a stable molecule with a large gap between the highest occupied (HOMO) and the lowest unoccupied molecular orbital (LUMO).[11] In $R_3N@C_{80}$, where R is a trivalent rare earth atom, this charge is obtained from the $R_3^{3+}N^{3-}$ endohedral cluster. Here we show that splitting of the C 1s core level of $TbSc_2N@C_{80}$ in high-resolution x-ray photoelectron spectroscopy (XPS) is related to the presence of the endohedral ions. The XPS data are quantitatively explained with density functional theory (DFT) calculations that yield lower C 1s eigenvalues for carbon atoms close to positively charged endohedral ions. The eigenvalues are correlated with the Coulomb potential of the endohedral unit at the carbon sites, which imposes an anisotropic Coulomb potential outside the carbon cages.

Results and Discussion

Figure 1(a) shows the Coulomb potential of a charge near a dielectric ($\epsilon = 3$).[12] The dielectric becomes polarised, though some field of the ion propagates into the dielectric, as can be seen from the electrostatic iso-potential contours. In a metal, where $\epsilon \to \infty$, the screening is complete and the situation of an ideal Faraday cage is met. At this stage it is not clear to which extent this picture of a continuum model describes the situation of a charge close to a single atom layer-material. The discreteness of the charges and the atomic lattice may involve polarisation in the form of an induced dipole *and* different charging of the carbon atoms that was predicted theoretically.[13]

Figure 1(b) displays the map of the electrostatic potential of $YSc_2N@C_{80}$ in the endohedral plane as calculated with DFT. We did the calculations with yttrium instead of terbium

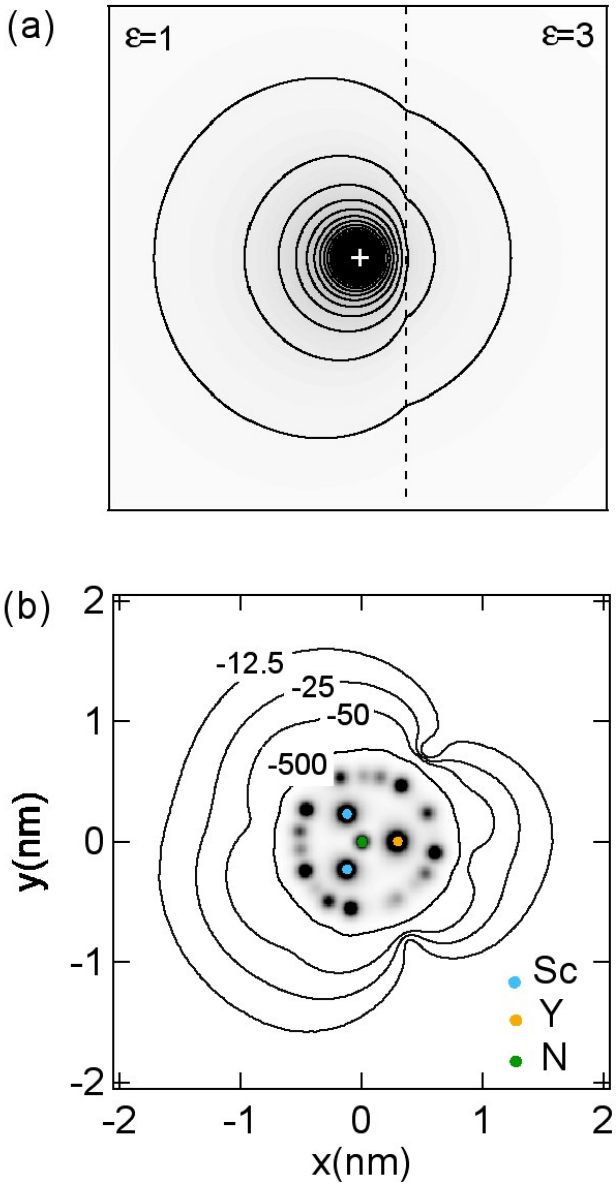

Figure 1: Electrostatic interaction across a dielectric interface. (a) Charge (+) in the vacuum ($\epsilon = 1$) in front of a dielectric ($\epsilon = 3$). The contours represent the iso-potentials in equal steps. The potential of the charge propagates into the dielectric, and if the latter is a layer, across it. (b) Coulomb potential of $YSc_2N@C_{80}$ on the plane given by the YSc_2 unit. The field exceeds the sphere that contains all molecular charge. The coordinate origin is set at the nitrogen nucleus (green). The rare earth ions are coloured in orange and light blue, the carbon atoms lie on a perimeter with 0.42 nm radius. The iso-potential contours are referred to the potential at infinity and given in meV.

because Y has the same valence, very similar size and electronegativity as Tb, but Y results are, due to the absence of a partially filled 4f shell, more reliable (cf Methods). Yttrium and scandium produce a different electrostatic potential *outside* the molecule. This information helps to understand the crystallisation behaviour of the molecules[8] and the interaction of the endohedral unit across the cage, which opens ways to electrostatically influence or control the endohedral orientation and magnetism.[10]

Figure 2 shows the comparison between the electrostatic potential at the positions of the 80 carbon atoms (a) and the corresponding C 1s eigenvalues of $YSc_2N@C_{80}$ (b). The atomic coordinates are taken from the DFT calculation. The Coulomb potential is calculated from three nominal $+3$ e charges at the positions of the rare earth ions and one -3 e charge at the site of the central nitrogen ion. From comparison of Figure 2(a) and (b) it becomes clear that the electrostatic potential shows the same trend as the eigenvalues: The carbon atoms in the vicinity of the rare earth ions have a lower electrostatic potential and lower eigenvalues. In order to compare the Coulomb potential of the endohedral unit U at the atomic carbon sites and the C 1s eigenvalues quantitatively they are plotted in Figure 3(a) and the correlation is evident. The eigenvalues have a spread ΔE of 1.01 eV. They reflect the electrostatic potential after screening due to the polarisation of the carbon shell, due to different charge on the carbon atoms and possible variations due to the two different carbon species in C_{80}. The majority species (C_{566} or corannulene carbon) is also encountered in C_{60}: 60 atoms sit on vertices where one pentagon- and two hexagon-faces meet. The minority species (C_{666} or pyrene carbon) consists of 20 atoms that sit on vertices where three hexagons meet (see inset in Figure 3(a)).[14] Both, the C_{566} and the C_{666} eigenvalues follow the Coulomb potential, where we find a slope $\Delta E : \Delta U$ of 0.15. The Coulomb potential variation ΔU of the nominal ionic charges in the cage is stronger than that of the eigenvalues ΔE. As we see from the Bader charge analysis[15] on all 84 atoms of the molecule, the DFT results produce in average an about 0.6 times smaller charging than the nominal assignment (e.g.+3 for Sc or -3 for N).[16] Furthermore, the screening of the potential at the carbon sites, i.e. the

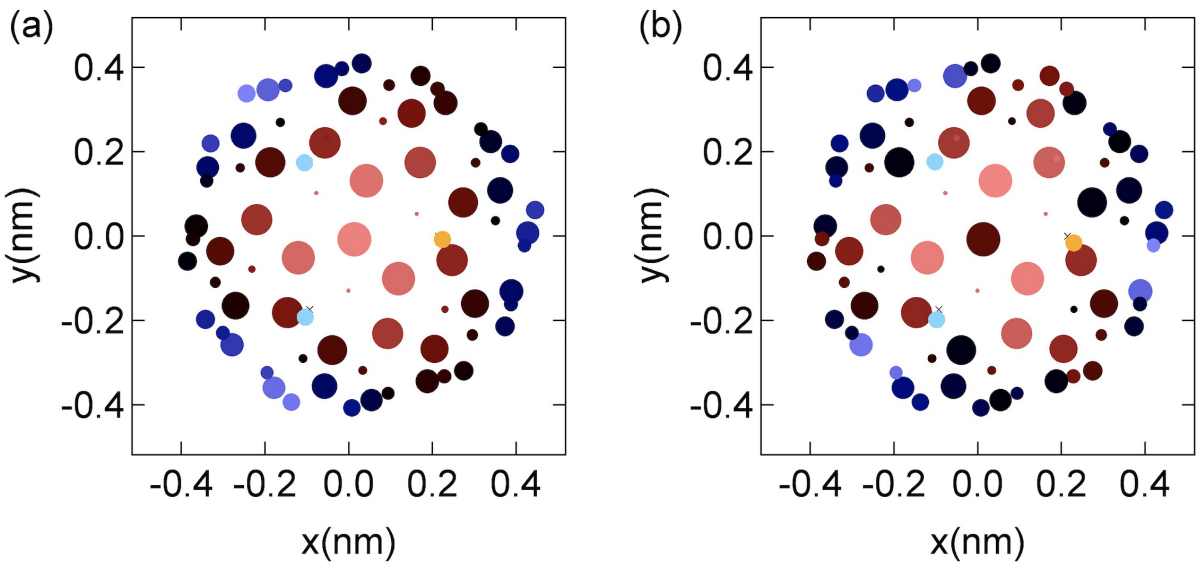

Figure 2: Comparison of (a) Coulomb potential of the YSc_2N endohedral unit at the 80 carbon sites and (b) calculated C 1s eigenvalues in $YSc_2N@C_{80}$ (red-black-blue circles). Blue sites attract electrons most. The size of the circles represents the z-coordinate and renders a perspective. As in Figure 1, the endohedral atoms Y (Sc) are depicted as orange (light blue) dots.

variation of the C 1s eigenvalues is affected by polarisation *and* different charge transfer on the individual carbon atoms. In Figure 3(b) the Bader charge on the 80 carbon atoms is plotted vs.. the Coulomb potential. The average Bader charge of -0.045 e per carbon atom is scattered in an interval of 0.2 e. This scatter indicates a significant electron reallocation on the carbon cage, which is related to the Coulomb potential of the endohedral ions. The offset between the C_{566} and the C_{666} eigenvalues of 343 meV is a chemical shift of different carbon species, where the lower eigenvalues of C_{666} are connected to a lower energy of the planar (pyrene) carbon. Although the lateral charge transfer on the carbon atoms does not support a classical polarisation picture, we are able to estimate an effective dielectric constant of the cage material from

$$\epsilon = \frac{n\ e}{2\epsilon_0}\frac{\Delta p}{\Delta E}\ , \tag{1}$$

where n is the areal dipole density on the carbon sphere, e the elementary charge, ϵ_0 the vacuum permittivity, and $\Delta p/\Delta E$ the slope of the dipole p vs. eigenvalue data. We recall

that this assumes the eigenvalues to follow the true electrostatic potential at the carbon cores and get with Equation 1 and all carbon atoms an effective ϵ of 2.0±0.2. The Bader dipole vs eigenvalue data show two more things: (i) The dipoles of the 6 carbon atoms (C_c) closest to the endohedral ions do not follow the trend of the others, because chemical interaction sets in and (ii) the corannulene carbons without the C_c's have a 70% larger effective ϵ than the pyrene carbons.

So far we have discussed theoretical results of the electric screening of the ions. Since the C 1s eigenvalues are reflected as well in core level photoemission binding energies, their comparison will test the theory. Figure 4 shows the C 1s eigenvalue spectrum of $YSc_2N@C_{80}$ and high resolution XPS data of the C 1s core level of a monolayer of $TbSc_2N@C_{80}$ on a hexagonal boron nitride nickel (h-BN/Ni(111))[17] surface. In the Methods section we give arguments why Y and Tb are considered to be equivalent for the present matters. Two peaks with an approximate 1:1 weight ratio are observed. This does not reflect the 3:1 ratio between C_{566} and C_{666} as seen in nuclear magnetic resonance[14] but has its origin in the charge distribution of the endohedral cluster. The eigenvalues were convoluted with a Gaussian of 380 meV full width at half maximum (FWHM) to account for the finite C 1s lifetime and the experimental resolution. This is in line with C_{60} where at room temperature the C 1s level has a FWHM of about 350 meV.[18] Furthermore, the theoretical energy scale is offset by 14.8 eV in order to match the experimental binding energies. This value accounts for the hole on the C 1s shell, which is left behind in the photoemission process but is not considered in the present ground state calculations. The agreement between theory and experiment is excellent, in particular the experimentally observed C 1s splitting is quantitatively reproduced. A posteriori this implies that Y and Tb must produce very similar electrostatics and that there are no strong additional energy differences among the 80 different photoemission final states. At this stage of comparison between experiment at 300 K and theory at 0 K the endohedral rotation[19] that sets in at around 50 K[20] does not impose a big change in the C 1s eigenvalue-distribution. In order to support this assessment

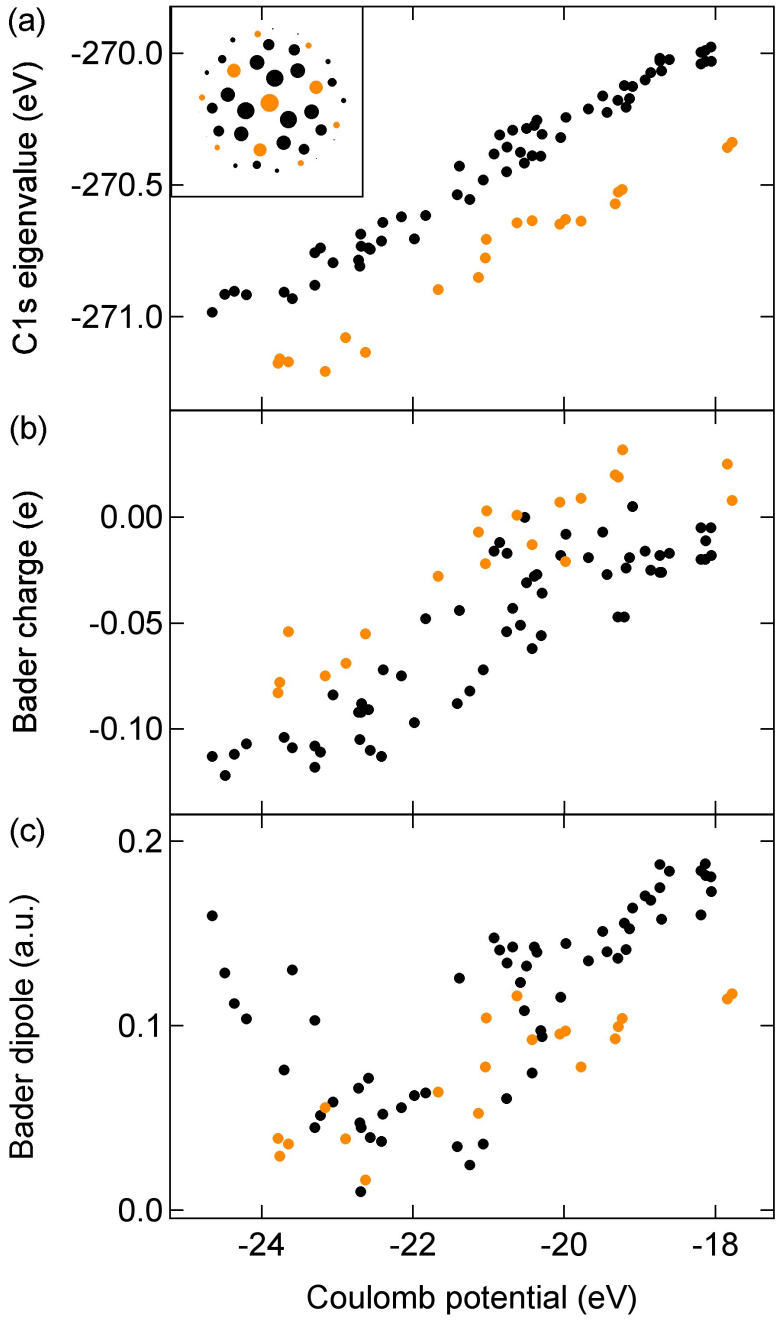

Figure 3: Correlation of the C 1s eigenvalues (a), the Bader charges on the carbon atoms (b), and the Bader dipole moments in atomic units (c), with the nominal Coulomb potential U of the endohedral unit on the positions of the 80 carbon atoms in $YSc_2N@C_{80}$. The black dots represent the 60 corannulene carbons C_{566} and the orange dots the 20 pyrene carbons C_{666} (see inset in (a)). (a) The eigenvalue calculations predict an average chemical shift of 343 meV between C_{566} and C_{666}. (b) The Bader charges indicate different electron affinities for corannulene and pyrene carbon. (c) The 6 corannulene carbons with low Coulomb potential have relatively large dipoles and signal the onset of chemical interaction.

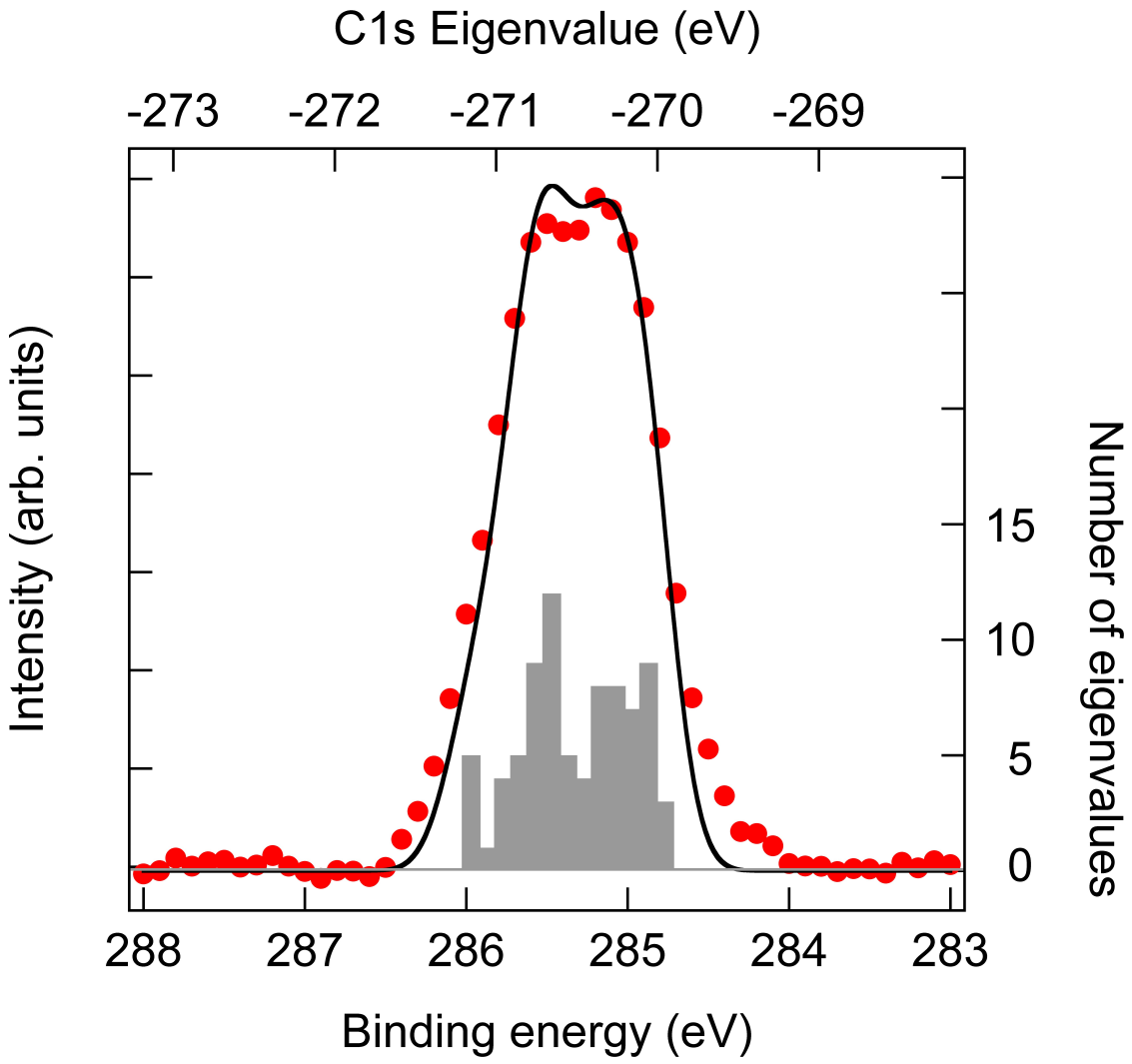

Figure 4: Comparison between calculated C 1s eigenvalues of $YSc_2N@C_{80}$ (grey bars and black line) and the high resolution x-ray photoelectron spectroscopy data of one monolayer $TbSc_2N@C_{80}$ on *h*-BN/Ni(111) (red dots). The eigenvalues span an energy range of 1.01 eV and are grouped in bins of 100 meV. The black line was obtained by convoluting the eigenvalues with a Gaussian of 380 meV full with at half maximum. The eigenvalues are offset to the experimental binding energies (by 14.8 eV), which accounts for the C 1s hole in the photoemission final state.

we show in the supplemental information eigenvalue spectra of three different endohedral conformations that are expected to be populated at room temperature.

The agreement between experiment and theory (Figure 4) and the correlation between Coulomb potential and C 1s eigenvalues (Figure 3(a)) demonstrates that the C 1s core level energy contains information on the interaction potential of ions across single layer carbon membranes.

Conclusions

In conclusion we traced back the peak splitting in the C 1s x-ray photoemission spectrum of $TbSc_2N@C_{80}$ on *h*-BN/Ni(111) to the C 1s eigenvalue distribution as obtained from density functional theory calculations. It was shown that the eigenvalues are correlated to the Coulomb potential of the endohedral unit. Analysis of the DFT results indicates laterally different charge distribution on the cage but an average effective dielectric constant ϵ of about 2 may be inferred, which identifies C_{80} as a non-ideal Faraday cage. From these findings we predict significant non-isotropic electric fields outside the molecule or behind any single layer membrane with finite ϵ and with adsorbed ions on one side. In the present case the electric fields are related to the endohedral cluster orientation, and they may be used for detecting and possibly addressing the endohedral orientation and magnetisation.

Acknowledgement

This work was supported by the Swiss National Science Foundation grant No. 200020_153312. Calculations were performed at the CSCS Swiss National Supercomputing Centre under project uzh11. The photoemission measurements were performed at the PEARL beamline of the Swiss Light Source, Paul Scherrer Institut, Villigen. AAP acknowledges the European Research Council (ERC) under the European Union Horizon 2020 research and innovation programme (grant No 648295 GraM3).

Methods

Theory

Since Tb^{3+} and Y^{3+} have the same formal charge, and very similar Shannon ionic radii (0.923 and 0.9 Å) and Pauling electronegativities (1.2 and 1.36), the DFT calculations were performed on the $YSc_2N@C_{80}$ endofullerene[21] rather than the lanthanide-containing $TbSc_2N@C_{80}$ because magnetic interaction may be neglected for the atomic structure, and yttrium is easier to handle theoretically and leads more reliable results with the present-day approximations to the exchange-correctional term in the Kohn-Sham single-particle equations. The calculations on the isolated $YSc_2N@C_{80}$ cluster were performed with the TurboMole code[22] and details are given in the supplemental materials.[16] They yield several possible orientations of the endohedral unit with very similar energies.[23] We checked the C_3, $C_{s,a}$ and $C_{s,b}$ in vacuum structures of $YSc_2N@C_{80}$.[16] In all these 3 configurations the endohedral YSc_2N unit is flat, i.e. the sum of the 3 pyramidal angles Sc_A-N-Sc_B, Sc_A-N-Y, and Y-N-Sc_B is 360°.[16] In the main text we show the results for the lowest-energy C_3 structure.

Experimental

$TbSc_2N@C_{80}$ with icosahedral I_h symmetry were synthesized and purified as described in Refs.[8,24] and sublimated onto h-BN/Ni(111).[17] As for C_{60}[25] this substrate does not impose a strong binding of the molecules to the substrate. The normal emission XPS data were recorded at room temperature and a photon energy of 600 eV. The overall energy resolution was below 200 meV.[26] The coverage was determined with a layer by layer growth model with an electron mean free path of 1 nm and from the intensity ratio of the N 1s core levels of the molecule and the hexagonal boron nitride substrate.[16]

Supporting Information Available

Supplemental Information: c1s_acs_sup.pdf including

- Theory
  - Details of density functional theory calculations
  - Coordinates and eigenvalues of $YSc_2N@C_{80}$
    - Structure C_3
    - Structure $C_{s,a}$
    - Structure $C_{s,b}$
    - Comparison of eigenvalue spectra C_3, $C_{s,a}$, $C_{s,b}$
- Experiment
  - Details of the sample preparation
  - Details of the measurements
  - Coverage determination with XPS

This material is available free of charge via the Internet at `http://pubs.acs.org/`.

References

(1) Almeida Murphy, T.; Th. Pawlik,; Weidinger, A.; Höhne, M.; Alcala, R.; J.-M. Spaeth, Observation of Atomlike Nitrogen in Nitrogen-Implanted Solid C_{60}. *Phys. Rev. Lett.* **1996**, *77*, 1075.

(2) Westerström, R.; Dreiser, J.; Piamonteze, C.; Muntwiler, M.; Weyeneth, S.; Brune, H.; Rusponi, S.; Nolting, F.; Popov, A.; Yang, S. et al. An Endohedral Single-Molecule Magnet with Long Relaxation Times: $DySc_2N@C_{80}$. *J. Am. Chem. Soc.* **2012**, *134*, 9840–9843.

(3) Delaney, P.; Greer, J. C_{60} as a Faraday cage. *Appl. Phys. Lett.* **2004**, *84*, 431–433.

(4) Sahin, H.; Topsakal, M.; Ciraci, S. Structures of fluorinated graphene and their signatures. *Phys. Rev. B* **2011**, *83*, 115432.

(5) Elias, D. C.; Gorbachev, R. V.; Mayorov, A. S.; Morozov, S. V.; Zhukov, A. A.; Blake, P.; Ponomarenko, L. A.; Grigorieva, I. V.; Novoselov, K. S.; Guinea, F. et al. Dirac cones reshaped by interaction effects in suspended graphene. *Nature Physics* **2011**, *7*, 701–704.

(6) Santos, E. J. G.; Kaxiras, E. Electric-Field Dependence of the Effective Dielectric Constant in Graphene. *Nano Letters* **2013**, *13*, 898–902.

(7) Popov, A. A.; Yang, S.; Dunsch, L. Endohedral Fullerenes. *Chem. Rev.* **2013**, *113*, 5989–6113.

(8) Stevenson, S.; Chancellor, C. J.; Lee, H. M.; Olmstead, M. M.; Balch, A. L. Internal and External Factors in the Structural Organization in Cocrystals of the Mixed-Metal Endohedrals ($GdSc_2N@I_h$-C_{80}, $Gd_2ScN@I_h$-C_{80} and $TbSc_2N@I_h$-C_{80}) and Nickel(II) Octaethylporphyrin. *Inorg. Chem.* **2008**, *47*, 1420–1427.

(9) Treier, M.; Ruffieux, P.; Fasel, R.; Nolting, F.; Yang, S.; Dunsch, L.; Greber, T. Looking inside an endohedral fullerene: Inter- and intramolecular ordering of $Dy_3N@C_{80}$ (I_h) on Cu(111). *Phys. Rev. B* **2009**, *80*, 081403.

(10) Westerström, R.; Uldry, A. C.; Stania, R.; Dreiser, J.; Piamonteze, C.; Muntwiler, M.; Matsui, F.; Rusponi, S.; Brune, H.; Yang, S. et al. Surface Aligned Magnetic Moments and Hysteresis of an Endohedral Single-Molecule Magnet on a Metal. *Phys. Rev. Lett.* **2015**, *114*, 087201.

(11) Nakao, K.; Kurita, N.; Fujita, M. Ab initio molecular-orbital calculation for C_{70} and seven isomers of C_{80}. *Phys. Rev. B* **1994**, *49*, 11415–11420.

(12) Jackson, J. D. *Classical electrodynamics*, 3rd ed.; Wiley: New York, NY, 1999.

(13) Popov, A. A.; Kaestner, C.; Krause, M.; Dunsch, L. Carbon Cage Vibrations of M@C_{82} and M_2@ C_{2n} (M = La, Ce; 2n=72, 78, 80): The Role of the Metal Atoms. *Fullerenes, Nanotubes and Carbon Nanostructures* **2014**, *22*, 202–214.

(14) Stevenson, S.; Rice, G.; Glass, T.; Harich, K.; Cromer, F.; Jordan, M. R.; Craft, J.; Hadju, E.; Bible, R.; Olmstead, M. M. et al. Small-bandgap endohedral metallofullerenes in high yield and purity. *Nature* **1999**, *401*, 55–57.

(15) Bader, R. F. W. *Atoms in Molecules - A Quantum Theory*, (international series of monographs on chemistry) ed.; Oxford, University Press: Oxford, 1990.

(16) See Supplemental Material at [URL will be inserted by publisher]: DFT total energy, coordinates, C 1s eigenvalues, Bader charges and dipoles for C_3, the total energies and coordinates of the $C_{s,a}$ and $C_{s,b}$ low energy structures, and experimental details.

(17) Auwärter, W.; Kreutz, T. J.; Greber, T.; Osterwalder, J. XPD and STM investigation of hexagonal boron nitride on Ni(111). *Surf. Sci.* **1999**, *429*, 229–236.

(18) Goldoni, A.; Cepek, C.; Larciprete, R.; Sangaletti, L.; Pagliara, S.; Paolucci, G.; Sancrotti, M. Core Level Photoemission Evidence of Frustrated Surface Molecules: A Germ of Disorder at the (111) Surface of C_{60} before the Order-Disorder Surface Phase Transition. *Phys. Rev. Lett.* **2002**, *88*, 196102.

(19) Fu, W.; Wang, X.; Azuremendi, H.; Zhang, J.; Dorn, H. C. 14N and 45Sc NMR study of trimetallic nitride cluster (M3N)6+ dynamics inside a icosahedral C80 cage. *Chemical Communications* **2011**, *47*, 3858.

(20) Kostanyan, A.; Westerström, R.; Zhang, Y.; Kunhardt, D.; Stania, R.; Büchner, B.; Popov, A. A.; Greber, T. Switching Molecular Conformation with the Torque on a Single Magnetic Moment. *Phys. Rev. Lett.* **2017**, *119*, 237202.

(21) Chen, N.; Fan, L.-Z.; Tan, K.; Wu, Y.-Q.; Shu, C.-Y.; Lu, X.; Wang, C.-R. Comparative spectroscopic and reactivity studies of $Sc_{3-x}Y_xN@C_{80}$ (x=0-3). *J. Phys. Chem. C* **2007**, *111*, 11823–11828.

(22) Ahlrichs, R.; Bar, M.; Haser, M.; Horn, H.; Kolmel, C. Electronic-Structure Calculations on Workstation Computers - The Program System TURBOMOLE. *Chem. Phys. Lett.* **1989**, *162*, 165–169.

(23) Yang, S.; Popov, A. A.; Dunsch, L. Carbon Pyramidalization in Fullerene Cages Induced by the Endohedral Cluster: Non-Scandium Mixed Metal Nitride Clusterfullerenes. *Angew. Chem. Int. Ed.* **2008**, *47*, 8196–8200.

(24) Zhang, Y.; Krylov, D.; Rosenkranz, M.; Schiemenz, S.; Popov, A. A. Magnetic anisotropy of endohedral lanthanide ions: paramagnetic NMR study of $MSc_2N@C_{80}$-Ih with M running through the whole 4f row. *Chem. Sci.* **2015**, *6*, 2328–2341.

(25) Muntwiler, M.; Auwärter, W.; Seitsonen, A. P.; Osterwalder, J.; Greber, T. Rocking-motion-induced charging of C_{60} on $h-$BN/Ni(111). *Phys. Rev. B* **2005**, *71*, 121402.

(26) Muntwiler, M.; Zhang, J.; Stania, R.; Matsui, F.; Oberta, P.; Flechsig, U.; Patthey, L.; Quitmann, C.; Glatzel, T.; Widmer, R. et al. Surface science at the PEARL beamline of the Swiss Light Source. *J. Synchrotron Radiat.* **2017**, *24*, 354.